

## Article

# Drought Stress Affects Spectral Separation of Maize Infested by Western Corn Rootworm

Raquel Peron-Danaher<sup>1,2,3</sup>, Lorenzo Cotrozzi<sup>1,3,4,†</sup> , Ali Masjedi<sup>3,4,‡</sup> , Laramy S. Enders<sup>1</sup> ,  
Christian H. Krupke<sup>1</sup>, Michael V. Mickelbart<sup>3,5</sup>  and John J. Couture<sup>1,3,4,\*</sup> 

<sup>1</sup> Department of Entomology, Purdue University, West Lafayette, IN 47906, USA; rperon@purdue.edu (R.P.-D.); lorenzo.cotrozzi@unipi.it (L.C.); lenders@purdue.edu (L.S.E.); ckrupke@purdue.edu (C.H.K.)

<sup>2</sup> Interdisciplinary Life Science Education Program, Purdue University, West Lafayette, IN 47906, USA

<sup>3</sup> Purdue Center for Plant Biology, Purdue University, West Lafayette, IN 47906, USA; amasjedi@purdue.edu (A.M.); mickelbart@purdue.edu (M.V.M.)

<sup>4</sup> Department of Forestry and Natural Resources, Purdue University, West Lafayette, IN 47906, USA

<sup>5</sup> Department of Botany and Plant Pathology, Purdue University, West Lafayette, IN 47906, USA

\* Correspondence: couture@purdue.edu

† Current address: Department of Agriculture, Food and Environment, University of Pisa, 56124 Pisa, Italy.

‡ Current address: Bayer Crop Science, St. Louis, MO 63141, USA.

**Abstract:** Root-feeding herbivores present challenges for insect scouting due to the reliance on above-ground visual cues. These challenges intensify in multi-stress environments, where one stressor can mask another. Pre-visual identification of plant stress offers promise in addressing this issue. Hyperspectral data have emerged as a measurement able to identify plant stress before visible symptoms appear. The effectiveness of spectral data to identify belowground stressors using aboveground vegetative measurements, however, remains poorly understood, particularly in multi-stress environments. We investigated the potential of hyperspectral data to detect Western corn rootworm (WCR; *Diabrotica virgifera virgifera*) infestations in resistant and susceptible maize genotypes in the presence and absence of drought. Under well-watered conditions, the spectral profiles separated between WCR treatments, but the presence of drought eliminated spectral separation. The foliar spectral profiles separated under drought conditions, irrespective of WCR presence. Spectral data did not classify WCR well; drought was well classified, and the presence of drought further reduced WCR classification accuracy. We found that multiple plant traits were not affected by WCR but were negatively affected by drought. Our study highlights the possibility of detecting WCR and drought stress in maize using hyperspectral data but highlights limitations of the approach for assessing plant health in multi-stress conditions.

**Keywords:** drought; hyperspectral data; maize; *Zea mays*; physiology; plant stress responses; Western corn rootworm



**Citation:** Peron-Danaher, R.; Cotrozzi, L.; Masjedi, A.; Enders, L.S.; Krupke, C.H.; Mickelbart, M.V.; Couture, J.J. Drought Stress Affects Spectral Separation of Maize Infested by Western Corn Rootworm. *Agronomy* **2023**, *13*, 2562. <https://doi.org/10.3390/agronomy13102562>

Academic Editors: Alvaro Fuentes, Chandra Shekhar Prabhakar and Dan Jeric Arcega Rustia

Received: 30 August 2023

Revised: 25 September 2023

Accepted: 27 September 2023

Published: 5 October 2023



**Copyright:** © 2023 by the authors. Licensee MDPI, Basel, Switzerland. This article is an open access article distributed under the terms and conditions of the Creative Commons Attribution (CC BY) license (<https://creativecommons.org/licenses/by/4.0/>).

## 1. Introduction

Over 4.5 billion people rely on maize as a primary source of food, especially in developing countries [1–3], and maize production has outpaced other cereals in these regions [4]. The current demand for maize production is increasing and is projected to need to double in the next 30 years to accommodate an increasing population (Rosegrant et al., 2009). Food demand is a massive challenge for maize producers and breeding programs, and the major limitations to increasing yield outputs are pests, pathogens, and environmental stress.

Western corn rootworm (WCR), *Diabrotica virgifera virgifera* LeConte (Coleoptera: Chrysomelidae), is a significant pest insect that challenges maize production in the United States [5] and is responsible for economic losses that can exceed USD 1–2 billion annually [6,7]. Root feeding by WCR larvae causes a considerable impact on maize

production, and it is estimated that every root node consumed by WCR larvae leads to a 20% reduction in yield [8]. WCR infestation also leads to plants lodging or falling over, which complicates mechanical harvesting and reduces yield output [9].

In North American maize production, WCR is managed primarily by using genetically modified maize varieties that produce a range of insecticidal proteins derived from the bacterium *Bacillus thuringiensis* (*Bt*). Extensive planting of *Bt* maize, however, increases the selection pressure for WCR that evolve resistance to *Bt* toxins [10]. Several studies have reported WCR resistance to *Bt* maize hybrids in most Western US corn belt states [9,11–13]. While most maize hybrids contain several genes that produce different *Bt* proteins as a strategy to reduce the likelihood of resistance evolving, there are no commercial maize genotypes fully resistant to WCR [13]. The most common approach for monitoring WCR in both nonmodified and *Bt* maize is manual scouting and scoring of root damage. These approaches, however, are time-consuming and limited by subjective assessments of plant status and scoring systems [14]. Moreover, early WCR infestation stages do not produce visual symptoms, and as a root-feeding herbivore, their life history makes a pre-visual diagnosis challenging [15].

In addition to pest insects, maize production experiences a wide variety of stressors, and drought is the leading abiotic cause of yield losses in maize [16]. Occurrences and areas affected by drought conditions are increasing globally, and the regions affected by drought doubled from 1970 to 2000 [16]. It has been hypothesized that WCR damage is intensified under water-limited conditions [17], yet most experimental manipulations of WCR densities or developmental stage and water conditions have shown that WCR has minimal impacts on maize in the presence of drought [18,19]. The influence of both stressors on the early detection of WCR, however, remains unclear.

One measurement approach that has become popular for assessing crop stress and health is hyperspectral data [14]. This approach has been successfully employed to detect pathogens and pests and understand the responses of vegetation to different stressors in numerous systems [20–34]. And although the detection of belowground pests and pathogens has been demonstrated [34–40], the ability of hyperspectral data to detect belowground stress using aboveground data in the presence of other stressors is unclear.

To address this knowledge gap, we tested the ability of hyperspectral data to detect WCR in WCR-susceptible and -resistant genotypes of maize exposed to the presence or absence of drought stress. Specifically, we predicted that hyperspectral data would be able to identify the presence of WCR prior to the onset of visible symptoms but that responses would vary between maize genotypes and water availability treatments. We also predicted that hyperspectral data would predict plant functional trait responses to WCR and drought treatments and that these responses would vary among maize genotypes and treatments.

## 2. Materials and Methods

### 2.1. Experimental Design and Germplasm

This study was conducted at Purdue University (40°42'26" N, 86°91'04" W, 611 m a.s.l.) in West Lafayette, IN, USA, in 2018 in two different types of controlled environments: the Ag Alumni Phenotyping Facility (AAPF) and a greenhouse (GH) in the Purdue Horticulture Plant Growth Facility. One genotype is characterized by the USDA as WCR-resistant (NGS; NGSDCRW1[S2]C4, Accession PI550643, repository N7) and the parental inbred, which is WCR-susceptible (R802; Accession Ames 30940, Repository N7).

#### 2.1.1. AAPF Experimental Design

In the AAPF, 96 plants, 48 each of the WCR-resistant (NGS) and the WCR-susceptible (R802) genotypes, were planted in a peat moss-based bark mix of BM7 soil (Berger, Saint-Modeste, QC, Canada) in 3 L plastic containers with drainage holes. We planted two seeds per container; after germination, one seedling was randomly removed, leaving only one plant per pot. The experiment was fertigated to full-volume capacity based on an automated, weight-based watering system. Fertigation included 150 ppm of 21-5-20 (N-P-K)

Peters Excel fertilizer (ICL Specialty Fertilizers, Dublin, OH, USA) and the chamber was maintained at 28:25 °C day:night temperatures. Each maize genotype was divided into two treatments: control (no WCR) and WCR-infested. To ensure sufficient root material was present for WCR establishment, WCR treatment plants were infested at the V4 (i.e., four fully developed leaf collars) stage with 100 WCR larvae per container in order to ensure a high infestation level. WCR eggs (Crop Characteristics, Farmington, MN, USA) were kept in a dark chamber at 27 °C until 50% of the eggs on the plate hatched. First instar WCR larvae were used to infest plants. For the infestation, the soil from the crown roots of individual plants was carefully removed, and WCR larvae were directly deposited on the crown roots with a Size 2 microdetail pain brush. The soil was then carefully replaced to cover the crown root area infested with WCR larvae. To increase the potential impact of WCR on the corn responses, measurements of all plants were conducted approximately 50 days at the V10 (i.e., ten fully developed leaf collars) stage.

### 2.1.2. GH Experimental Design

Seeds of the same genotypes used in the AAPF experiment were planted in a growing medium containing a 1:1 mixture of Berger special mix, a custom blend of BM7 and BM8 (Berger, Saint-Modest, QC, Canada), in 7.5 L black plastic containers with drainage. The number of containers per genotype planted was 120, for a total of 240 pots. Containers were regularly fertigated to pot capacity using N-P-K-enriched water (400 ppm of 21-5-20 N-P-K Peters Excel fertilizer, ICL Specialty Fertilizers, Dublin, OH, USA) throughout the entire experiment, and the greenhouse was maintained at 25:22 °C day:night temperatures.

Plants were subdivided into two sets following a randomized, complete block design, each composed of 120 seedlings per genotype, and sub-assigned to four different treatments: control (well-watered, non-WCR-infested); well-watered, infested with WCR; drought stress; and drought stress infested with WCR. For WCR infestations, sixty plants of each genotype were infested at the V4 stage with 100 WCR first instar larvae (Crop Characteristics, Farmington, MN, USA), similar to the protocol described in the AAPF experiment. To implement drought treatments, all plants were regularly watered until the V6 plant stage. Plants were considered to be under drought stress by measuring the photosynthetic and stomatal conductance levels to a level of 30% below the well-watered plants. After this period, water was withheld from the two drought treatments (i.e., drought and drought + WCR) for nine days, while the two well-watered groups were irrigated every two days to capacity. At the time of the measurements (approximately 50 days after planting), all plants were at the V10 stage.

### 2.2. Spectral Data Collection and Calculation of Indices

Full-range (350–2500 nm) reflectance profiles were obtained using a spectroradiometer (Spectral Vista Corporation, Poughkeepsie, NY, USA) fitted with a leaf clip containing an internal halogen light source. In the AAPF experiment, spectral measurements were made on two different areas on opposite sides of the leaf midvein, midway between the leaf tip and collar of the adaxial surface of all possible leaves, which were averaged to one spectral measurement per plant. For the GH experiment, three different areas of the adaxial surface in each V7 leaf were measured and then averaged following [30]. The relative reflectance of each leaf was determined using the leaf radiance divided by the radiance of a white reference panel internal to the leaf clip, measured every 15 spectral collections. Several vegetation indices (Vis) were calculated using the spectral data collected at both experiments described in the literature to be related to abiotic and biotic stress (Table 1).

We also calculated the Normalized Differential Spectral Index (NDSI) for all pairwise wavelength combinations following  $NDSI [i, j] = \frac{R_i - R_j}{R_i + R_j}$ , where  $R$  is the reflectance value of the respective wavelengths. Spearman rank correlations were used to determine relationships between pairwise wavelength combinations and treatment combinations following [25]. This approach allows for the identification of wavelengths, or combinations of wavelengths, related to the treatments or plant responses to the treatments.

**Table 1.** Vegetation indices, formulas, biological parameter estimated, and reference for the calculations used in the current study.

Index	Name	Formula	Estimated Parameter	Reference
PRI	Photochemical Reflectance Index	$(R531 - R570)/(R531 + R570)$	Photosynthesis	[41]
NDWI	Normalized Difference Water Index	$(R860 - R1240)/(R860 + R1240)$	Leaf water content	[42]
DSWI	Disease Water Index	$R800/R1660$	Detect specific disease and pests	[43]
PBI	Plant Biochemical Index	$R810/R560$	Plant biochemicals	[44]
ARI	Anthocyanin Reflectance Index	$(1/R550) - (1/R700)$	Pigments	[45]
HI	Health Index	$(R534 - R698)/(R534 + R698) - \frac{1}{2} \times (R704)$	Vegetation health	[46]
WBI	Water Band Index	$R970/R902$	Plant water relation	[47]
MCARI	Modified Chlorophyll Absorption Reflectance Index	$[(R700 - R670) - 0.2 \times (R700 - R550)] \times (R700/R670)$	Chlorophyll Green Leaf Area Index	[48]

### 2.3. Maize Physiological Reference Measurements

Reference measurements were collected on plants in the GH experiment immediately following the spectral measurements. The 7th leaf of each plant was consecutively measured once for the chlorophyll content, gas exchange parameters, and water relations on the leaf on which spectral data were collected. All measurements were performed between 10:00 a.m. and 3:00 p.m.

#### 2.3.1. Chlorophyll Content and Gas Exchange

The chlorophyll content (SPAD) was measured using a digital chlorophyll meter analyzer (SPAD 502 m, Konica Minolta, Tokyo, Japan). The net CO<sub>2</sub> assimilation (A), stomatal conductance (g<sub>s</sub>), intercellular CO<sub>2</sub> concentration (C<sub>i</sub>), transpiration (Transp), and temperature of the adaxial leaf surface was measured using an LI-6400XT portable photosynthesis system (LiCor, Inc., Lincoln, NE, USA) with 400 ppm CO<sub>2</sub> and saturated light (1700 μmol m<sup>-2</sup> s<sup>-1</sup> photosynthetically active radiation). We calculated the intrinsic water use efficiency (WUE) as A divided by g<sub>s</sub>.

#### 2.3.2. Water Status and Leaf Thickness

The leaf water potential (Ψ<sub>w</sub>) was measured using a 10–15 cm portion of the leaf. The leaf midvein was placed into a rubber stopper and inserted into a Scholander pressure chamber (Model 600; PMS Instrument, Company, Corvallis, OR, USA), as described by Tiekstra et al. (2000). A portion of the leaf lamina directly subtending the tissue used to measure the Ψ<sub>w</sub> was used to determine the leaf osmotic potential (Ψ<sub>π</sub>). The leaf was placed in a microcentrifuge tube with a mesh insert, quickly frozen in liquid nitrogen, then stored at −20 °C. The samples were removed from the freezer and kept for ten minutes at room temperature, then centrifuged for 5 min at 500 rpm to extract the cell sap. The solute concentration was quantified using a vapor pressure osmometer (Wescor 5500; Wescor Inc., Logan, UT, USA) following [49]. Using another portion of the leaf, the relative water content (RWC) and leaf succulence (Succ) were measured following the protocol described by [49]. The RWC was determined using the formula FW-DW/TW-DW (FW: fresh weight, DW: dry weight, and TW: turgid weight). The leaf portion used for RWC was scanned to obtain the leaf area (LA) using a Canon Lide 300 scanner (One Canon Park, Melville, NY, USA). The leaf area was quantified using ImageJ (National Institutes of Health, Bethesda, MD, USA), and the mass was weighed to calculate the SLA.

### 2.4. Chemometric Modeling

Chemometric models were developed to predict several traits in maize in the GH experiment, including the net CO<sub>2</sub> assimilation (A), transpiration (Transp), stomatal conductance (g<sub>s</sub>), intercellular CO<sub>2</sub> concentration (C<sub>i</sub>), relative water content (RWC), intrinsic water use efficiency (WUE), leaf greenness (SPAD), leaf temperature (T<sub>leaf</sub>), leaf water potential (LWP), leaf osmotic potential (LOP), and specific leaf area (SLA). Models were developed using partial least squares regression (PLSR) [50,51]. PLSR is a common approach for developing models estimating plant traits using spectral data, because the approach reduces the multicollinearity within spectral data into uncorrelated latent variables [30,52].

The number of latent variables for each model was selected based on the reduction of the predicted residual error sums of squares (PRESS) statistic [53] using the leave-one-out (LOO) cross-validation approach. All the models were developed using the wavelength range from 400 to 2400 nm. A maximum of fifteen percent of data were removed as outliers, based on [30], for each trait modeled, but the data points removed varied by the individual trait modeled. The model performance was evaluated by conducting 100 randomized permutations of the dataset using 80% of the data ( $n = 192$ ) divided into an 80:20 split for calibration and cross-validation, respectively. The 20% of the remaining data ( $n = 48$ ) was held onto to perform external validation. To determine the model performance, we tracked the model's goodness of fit ( $R^2$ ) and overall error rate (root mean square error, RMSE), the error normalized to the data range (NRMSE), and the bias for each permutation. Models that performed satisfactorily (i.e., external validation  $R^2 > 0.65$  and NRMSE  $< 20\%$ ) were used to predict physiological traits in the AAPF experiment and for further analysis of these traits in the treatments.

### 2.5. Root Injury Assessment

Following the data collection for both experiments, all plant roots were extracted and thoroughly rinsed to remove soil. WCR damage was assessed using the root node injury scale developed by [54]. This approach is a quantitative assessment of root injury caused by WCR larvae feeding. The scale scoring goes from zero (i.e., no feeding damaged) to three (i.e., three or more complete nodes pruned).

### 2.6. Statistical Analyses

Analysis of variance (ANOVA) was performed to determine the effect of treatment combinations on root damage. Data collected from the AAPF experiment were analyzed as a two-way ANOVA with the main effects of WCR infestation, genotype, and their interaction following the model  $W_{i,j} = W_i + G_j + W_iG_j + e_{i,j}$ . In this model,  $W_i$  represents the WCR treatment level  $i$ ,  $G_j$  represents the genotype level  $j$ , and  $e_{i,j}$  represents the error term. A three-way ANOVA following a similar model was used for analysis of the data collected in the greenhouse experiment, except the term  $D_j$  was included to account for the presence or absence of drought and was included both individually and through interactions with other factors.

Two approaches were used to identify the influence of treatments on spectral profiles: dissimilarity analysis and classification. For both analyses, the data ranges of 500 to 800 nm and 1600 to 2200 nm were used. Those ranges were selected because those wavelength ranges contain absorption features related with biotic stress responses based on the red edge position, changes in the pigment profiles, and phenolic absorption features (Curran et al., 1989; Kokaly and Skidmore 2015; Cotrozzi and Couture 2020; Galiene et al., 2021).

In the AAPF and GH experiments, permutational multivariate analysis of variance (PERMANOVA, [55]) was the dissimilarity analysis performed using Euclidian distance measurements and 10,000 permutations to determine if (1) the WCR, genotype, or their interaction had an influence on the dissimilarity of the spectral data (AAPF) and (2) the WCR, drought, genotype, or their interactions had an influence on the dissimilarity of the spectral data (GH). We visualized the dissimilarities using principal coordinate analysis (PCoA) with Euclidian distance measurements. Both PERMANOVA and PCoA were performed in R using the package "vegan" ([www.r-project.org](http://www.r-project.org), Dixon, 2003, accessed on 15 February 2019). If a treatment factor was found to be statistically significant for the PERMANOVA, a least significant difference post hoc test was performed on the first PCoA axis. We then proceeded to the classification analysis of the treatments using the spectral data by applying a support vector machine (SVM) classification analysis. SVM is a supervised classification approach where hyperplanes are used to separate samples using known identifiers in a training dataset and then outcomes derived from the training set are used to predict the identifier in a validation dataset [56]. The ability of SVM to discriminate nonlinear data relationships using the kernel function makes it an optimal classification

approach for high-dimensional, multivariate, non-independent datasets [56]. We used the open python resource Jupiter notebook to perform the SVM analysis. The dataset was split 50:50 for the training and validation datasets. We analyzed the training data using a k-fold ( $k = 10$ ) resampling approach.

ANOVA was performed separately for each experiment to determine the effect of treatment combinations on individual VIs and functional traits using a similar model as used for the root damage assessment. Because of the small sample sizes of some of the treatments and to balance between potential type I and II errors, we report  $p$ -values  $p > 0.05$  as significant and  $p$ -values  $0.05 \leq p \leq 0.10$  as marginally significant [57].

### 3. Results

#### 3.1. Root Injury Assessment

Both resistant and susceptible genotypes experienced feeding damage by WCR (AAPF treatment, Appendix A, Figures A1 and A2). We found that the WCR-susceptible genotype had higher root damage in both experiments compared to the resistant genotype (Appendix A, Figures A1 and A2). Drought had no influence on WCR damage for the greenhouse experiment (Appendix A, Figure A2).

#### 3.2. Spectral Separation and Classification among Different Treatment Combinations

In the AAPF experiment, we found that composite spectral profiles separated independently for both the WCR treatments and between genotypes, but we found no interaction between the two factors (Figure 1a and Appendix B, Table A1). Full spectral profiles separated more between genotypes, especially in the SWIR region (Figure 1b). In the GH experiment, we found that composite spectral profiles separated between genotypes and drought treatment but not WCR (Figure 1c and Appendix B, Table A1). Instead, the separation of composite spectral profiles of plants infested and not infested with WCR was influenced by the presence of drought stress (WCR  $\times$  drought interaction, Figure 1c and Appendix B, Table A1), and the separation of composite spectral profiles of different genotypes depended on the presence or absence of drought stress (genotype  $\times$  drought interaction, Figure 1c and Appendix B, Table A1). Similar to the AAPF, full spectral profiles separated more between genotypes, with treatment responses occurring largely in the SWIR region (Figure 1d).

SVM showed low accuracy in classifying plants infested with WCR in both experiments using spectral data (Figure 2a,b). In the AAPF, the classification of non-WCR and WCR treatments was similar, with a ~50% classification accuracy (Figure 2a). Similar to the AAPF outcome, spectral data collected in the GH experiment did not classify WCR well, again with ~50% classification accuracy (Figure 2b). When including all treatment combinations, classification showed reduced accuracy for all categories (Figure 2d).

#### 3.3. Relationships between the Normalized Differential Spectral Index (NDSI), Treatment Combinations, and Vegetation Indices (VI)

Using the NDSI, the relationships of spectral data with treatment combinations revealed weaker relationships of spectral data with WCR (Figure 3a,b) than with drought (Figure 3c). In the AAPF experiment, PBI and MCARI were the only indices related to WCR infestation (Table 2), with PBI being 6% lower and MCARI 13% higher in the WCR treatments (Appendix B, Table A2). The PRI, NDWI, PBI, HI, and WBI varied between genotypes, but we found no WCR  $\times$  genotype interactions (Table 2). In the GH experiment, we found that the PBI and DSWI were the only indices related with WCR infestation (Table 2). Again, PBI was 6% lower in WCR-infested plants, while DSWI was 5% lower (Table 1 and Appendix B, Table A2). The magnitude of this response depended on drought levels but was consistent across genotypes (Table 2). In the GH experiment, all VIs except the MCARI responded to drought (the PRI and WBI increased 32% and 3%, respectively, and the NDWI, DSWI, PBI, ARI, and HI decreased by 7%, 13%, 12%, 16%, and 60%, respectively,

Appendix B, Table A2), although several of these responses varied between genotypes (drought × genotype interaction; Table 2).

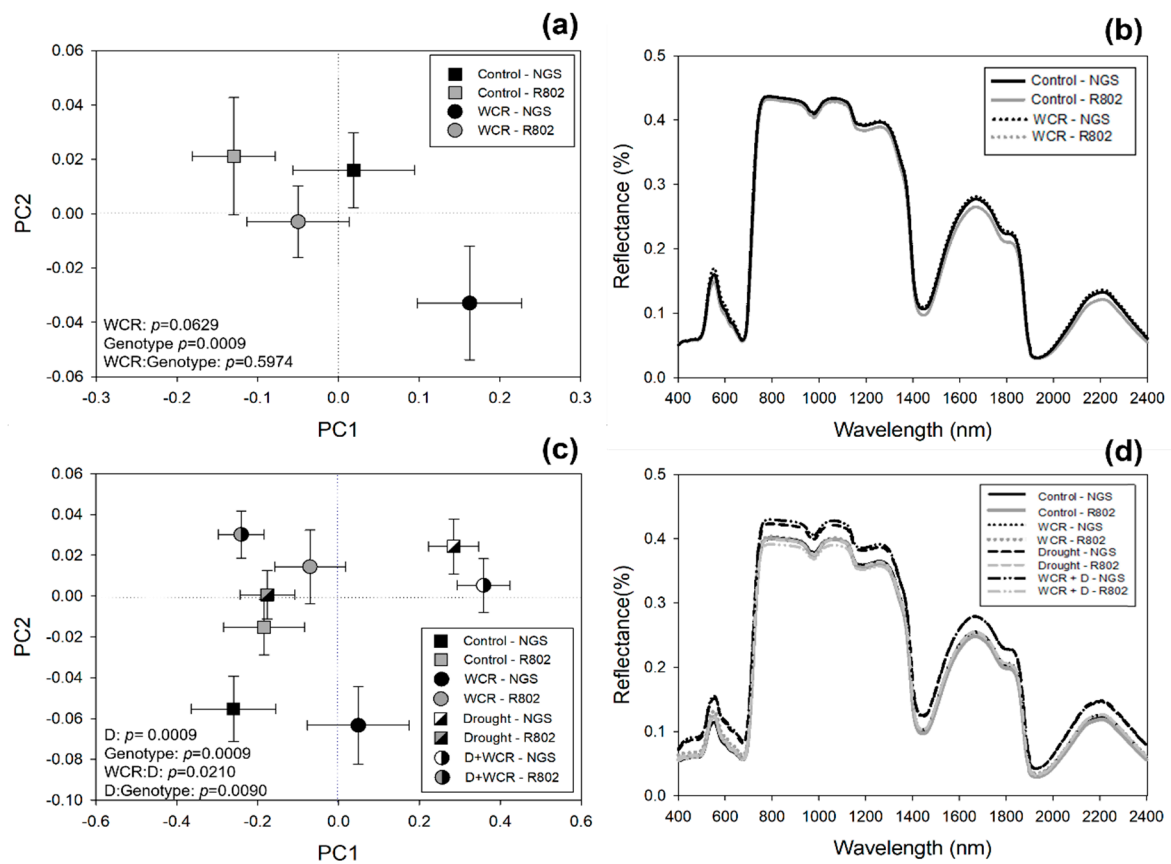


**Figure 1.** Principal coordinate analysis (PCoA; a,c) and spectral profile (b,c) of composite spectral profiles among treatments in the AAFP (a,b) and the GH (c,d) experiments. Permutational analysis of variance (PERMANOVA) results reported as pseudo *p*-values. Only *p*-values < 0.10 are displayed. Scores (mean ± standard error) for the first and second vectors from PCoA of hyperspectral data collected from both experiments: (a,b) AAFP experiment and (c,d) GH experiment. WCR: Western corn rootworm; D: drought; D + WCR: drought + WCR; NGS: maize genotype resistant to WCR; R802: maize genotype susceptible to WCR.

**Table 2.** *p*-values of two- and three-way ANOVA examining the effects of Western corn rootworm (WCR) infestation, genotype, and their interaction (AAFP) or WCR, drought, genotype, and their interactions (GH) on VI responses. Significant values (*p* < 0.05) are in bold, while marginally significant values (0.10 ≤ *p* ≤ 0.05) are italicized. *df*, degrees of freedom (numerator, denominator). AAFP: Ag Alumni controlled environment Phenotyping Facility. GH: greenhouse. PRI: Photochemical Reflectance Index, NDWI: Normalized Difference Water Index, DSWI: Disease Severity Water Index, PBI: Plant Biochemical Index, ARI: Anthocyanin Reflectance Index, HI: Health Index, WBI: Water Band Index, MCARI: Modified Chlorophyll Absorption in Reflectance Index.

Experiment	Treatment	<i>df</i>	PRI	NDWI	DSWI	PBI	ARI	HI	WBI	MCARI
AAFP	WCR	1,89	0.460	0.339	0.799	<i>0.055</i>	0.475	0.290	0.315	<b>0.024</b>
	Genotype	1,89	<b>&lt;0.001</b>	<b>&lt;0.001</b>	0.300	<b>0.002</b>	0.333	<i>0.056</i>	<b>&lt;0.001</b>	0.491
	WCR × genotype	1,89	0.323	0.447	0.450	0.590	0.291	0.720	0.868	0.148
GH	WCR	1,237	0.210	0.637	<i>0.068</i>	<b>0.007</b>	0.226	0.146	0.921	0.247
	Drought	1,237	<b>&lt;0.001</b>	<b>0.006</b>	<b>&lt;0.001</b>	<b>&lt;0.001</b>	<b>0.006</b>	<b>&lt;0.001</b>	<b>0.003</b>	0.445
	Genotype	1,237	<b>&lt;0.001</b>	0.450	<b>&lt;0.001</b>	<b>0.045</b>	0.541	<b>&lt;0.001</b>	<i>0.093</i>	<i>0.076</i>
	WCR × drought	1,237	0.545	0.928	0.047	<i>0.077</i>	0.431	<i>0.073</i>	0.582	0.717
	WCR × genotype	1,237	0.438	0.390	0.567	0.714	0.777	0.380	0.206	0.490
	Drought × genotype	1,237	<b>&lt;0.001</b>	0.343	<b>0.004</b>	<b>&lt;0.001</b>	<b>&lt;0.001</b>	<b>&lt;0.001</b>	0.374	0.230
	WCR × drought × genotype	1,237	0.841	0.462	0.756	0.682	0.578	0.842	0.556	0.230

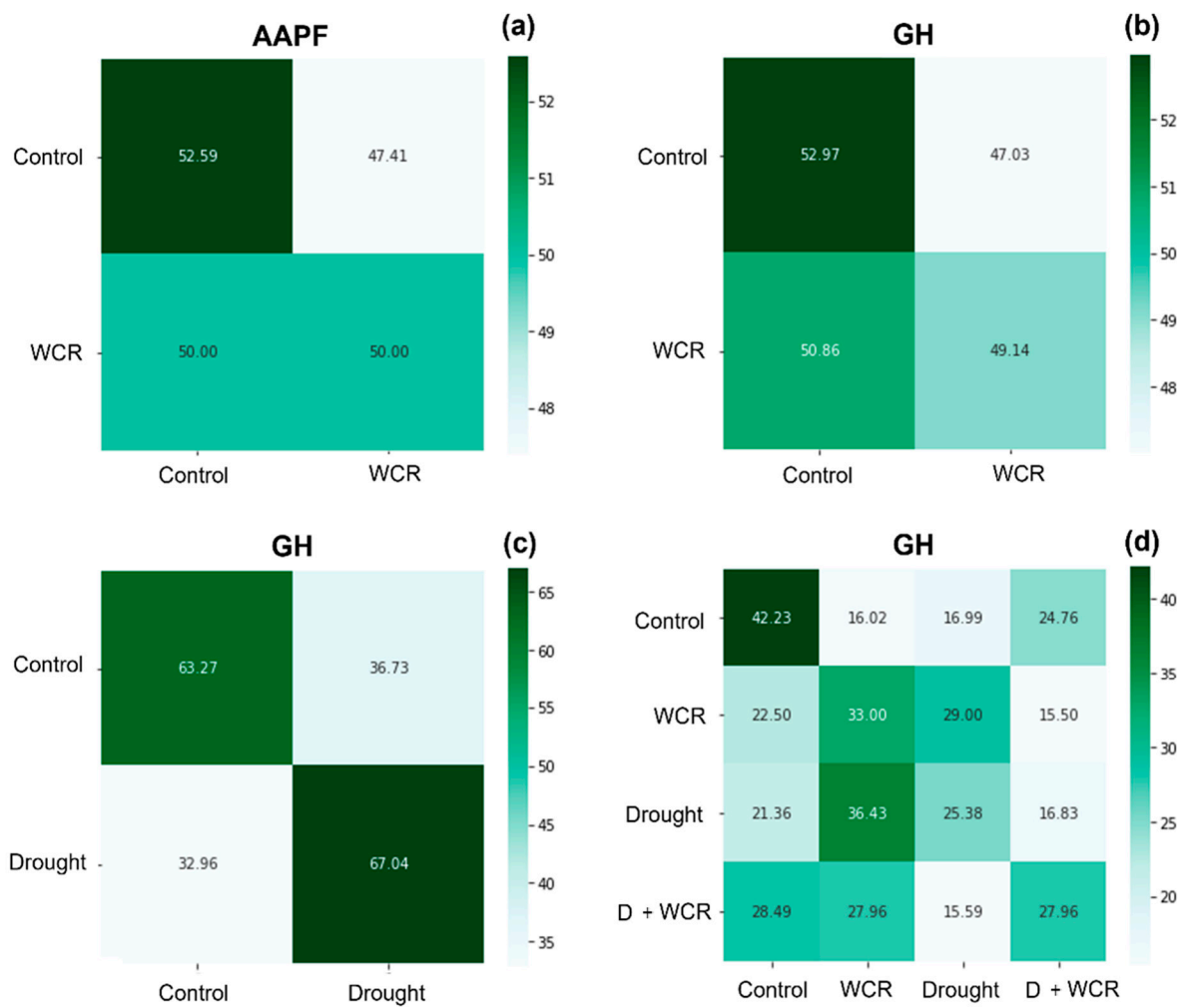


**Figure 2.** Classification matrix for AAPF and GH experiments showing the classification accuracy of the treatment combinations in both experiments. (a) AAPF experiment and (b–d) GH experiment. Treatment description: control; WCR: Western corn rootworm; D: drought; D + WCR: drought + WCR.

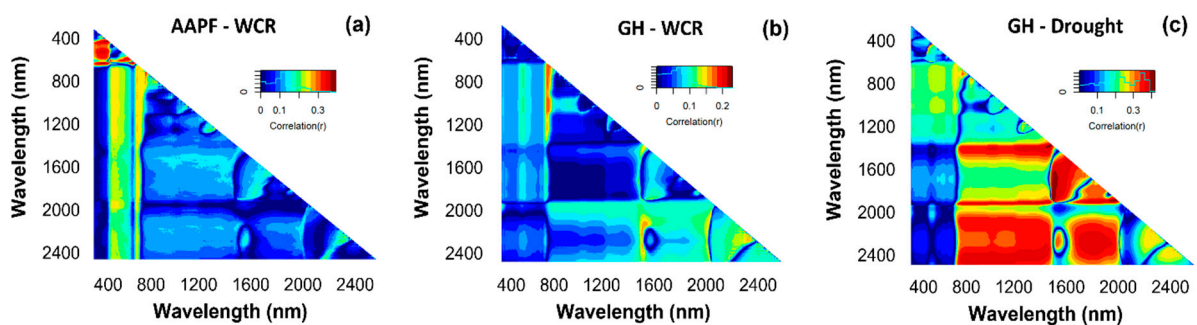


**Figure 3.** Normalized Differential Spectral Index (NDSI) of all possible combinations of the full spectral range (400–2400 nm), showing relationships of wavelengths with WCR treatments at AAPF (a) and WCR (b) and drought (c) in the greenhouse (GH).

Overall, the NDSI showed weaker relationships for spectral data with the PBI and DSWI for all treatments in the AAPF compared to the GH experiment (Figure 4a–d). There was approximately a 70% reduction in the total number of correlation coefficients that were >0.5, but a seven- and five-fold reduction in correlation coefficients that were >0.7, for spectral data with the PBI and DSWI in the AAPF (Figure 4a,c) compared to the GH (Figure 4b,d). We also found more prominent relationships of NDSI values relating spectral

data in regions containing water absorption features (i.e., 970–1450 nm and 1920–2172 nm; Figure 4b,d) in the GH experiment compared to the AAPF and in the drought compared to the WCR treatments in the GH, indicating a more pronounced impact of drought stress than WCR on vegetation spectral profiles.

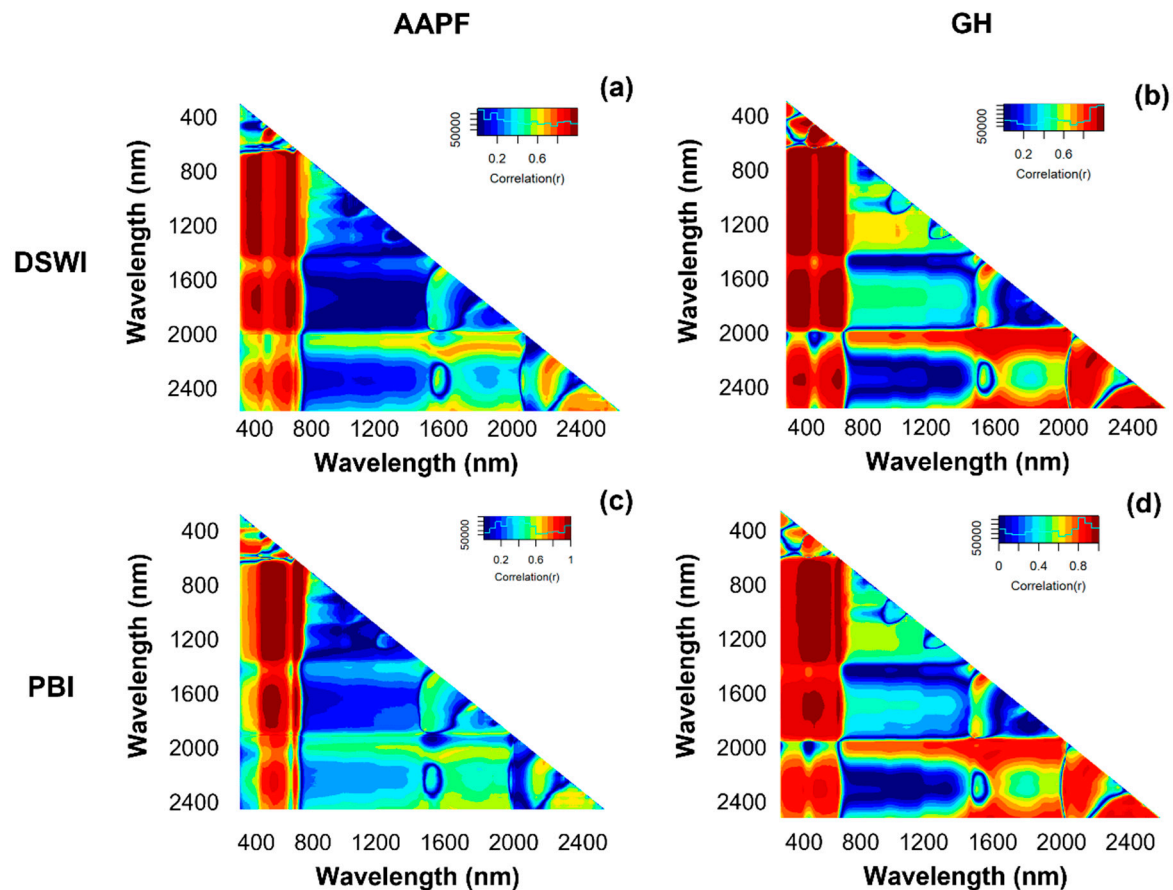


**Figure 4.** Heat maps relating the normalized differential spectral indices generated using the spectral range 400–2400 nm related to all treatments using the Disease Severity Water Index (DSWI) and the Plant Biochemical Index (PBI) calculated from leaf spectral collections in the AAPF (a,c) and GH (b,d) experiments.

### 3.4. Functional Traits

Many of the spectral models we developed to estimate physiological traits performed well (Appendix B, Table A3). Specifically,  $A$ ,  $Transp$ ,  $g_s$ ,  $C_i$ ,  $RWC$ ,  $Tleaf$ , and  $SLA$  all demonstrated  $R^2$  values  $\geq 0.65$  and error rates below  $\leq 20\%$  (Appendix B, Table A3). These models were retained for further examination of the impact of WCR and drought on maize physiological responses.  $WUE$ ,  $SPAD$ ,  $LWP$ , and  $LOP$  all performed more poorly than expected, with either  $R^2 < 0.50$ , error rates greater than 20%, or both, and were not included in further analyses.

The leaf temperature was the only response to WCR detected in the AAPF experiment, but the response depended on the genotype, with the leaf temperature of the susceptible genotype being 7% higher than the resistant genotype (WCR  $\times$  genotype interaction; Table 3 and Appendix B, Table A4). The  $SLA$  did vary between genotypes in the AAPF experiment, but the response was only marginally significant in the GH study (Table 3 and Appendix B, Table A4). In the GH experiment, we found no direct influence of WCR on any functional traits, but the WCR presence did increase the  $SLA$  to levels comparable with drought (marginal WCR  $\times$  drought interaction; Table 3 and Appendix B, Table A4). Drought had a more pronounced influence on the physiological responses than WCR and reduced assimilation and transpiration by 67%, stomatal conductance by 54%,  $RWC$  by

17%, and increased the SLA by 9% in the GH study (Table 3 and Appendix B, Table A4); the magnitude of these responses, however, varied among genotypes (Table 3 and Appendix B, Table A4).

**Table 3.** *p*-values of two- and three-way ANOVA examining the effects of Western corn rootworm (WCR) infestation, genotype, and their interaction (AAPF) or WCR, drought, genotype, and their interactions (GH) on functional trait responses. Significant values ( $p < 0.05$ ) are bolded, while marginally significant values ( $0.10 \leq p \leq 0.05$ ) are italicized. *df*, degrees of freedom (numerator, denominator); AAPF, Ag Alumni controlled environment Phenotyping Facility; A, net CO<sub>2</sub> assimilation; Transp, transpiration; *g*<sub>s</sub>, stomatal conductance; C<sub>i</sub>, intercellular CO<sub>2</sub> concentration; RWC, relative water content; T<sub>leaf</sub>, leaf temperature.

Experiment	Treatment	<i>df</i>	A	Transp	<i>g</i> <sub>s</sub>	C <sub>i</sub>	RWC	T <sub>leaf</sub>	SLA
AAPF	WCR	1,89	0.178	0.115	0.115	0.229	0.195	0.710	0.457
	Genotype	1,89	0.380	0.852	0.938	0.977	0.410	<b>&lt;0.001</b>	<b>0.004</b>
	Genotype × WCR	1,89	0.424	0.716	0.536	0.756	0.932	<b>0.027</b>	0.628
GH	WCR	1,237	0.851	0.809	0.187	0.187	0.306	0.409	0.291
	Drought	1,237	<b>&lt;0.001</b>	<b>&lt;0.001</b>	<b>&lt;0.001</b>	<b>&lt;0.001</b>	<b>&lt;0.001</b>	0.956	<b>0.001</b>
	Genotype	1,237	<b>&lt;0.001</b>	<b>&lt;0.001</b>	<b>&lt;0.001</b>	<b>&lt;0.001</b>	<b>&lt;0.001</b>	0.486	0.107
	WCR × Drought	1,237	0.152	0.139	<i>0.056</i>	<i>0.056</i>	0.570	0.956	<i>0.081</i>
	WCR × Genotype	1,237	0.277	0.638	0.354	0.354	0.813	0.563	0.284
	Drought × Genotype	1,237	<b>&lt;0.001</b>	<b>&lt;0.001</b>	<b>&lt;0.001</b>	<b>&lt;0.001</b>	<b>&lt;0.001</b>	0.978	0.997
	WCR × Drought × Genotype	1,237	0.699	0.970	0.675	0.675	0.680	0.810	0.460

#### 4. Discussion

Detecting plant stress prior to the onset of visual symptoms is a management approach that can dramatically drive crop yield improvement [32,58–60]. Plants exposed to different stressors can respond by activating a series of complex signaling networks [58]; however, accurately assessing plant stress pre-visually can be challenging when there are multiple sources of stress interacting simultaneously [30]. Hyperspectral data have proven to be an effective method to assess plant abiotic and biotic stress pre-visually in aboveground tissue when the occurrence of stress is present [25,40,56,61–64]. In addition, there is building evidence that aboveground spectral data can detect the presence of belowground pests or pathogen stress [35–40]. The influence of multiple stress events on the ability of spectral data to detect the presence of belowground pests or pathogens using aboveground measurements, however, is not well understood and represents a limitation in the utility of the approach. In this study, we found that changes in the composite spectral profile of plants infested with WCR were detected in a controlled environment and in the absence of drought stress. We also found that the presence of drought seemed to mask the separation of composite spectral profiles of plants infested with WCR. Lastly, the VIs calculated and physiological traits measured produced stronger responses and correlated more with drought stress than WCR infestation. The results of our study highlight the limitations in detecting multiple stress events using hyperspectral data.

An emergent outcome of this work is that the presence of multiple stressors can influence the ability of spectral data to detect an individual stress event, especially if one of the stress events does not produce a sufficiently measurable response. Regardless of the separation of the composite spectral profiles among treatments, we found poor outcomes when classifying the WCR presence individually, and classification was further reduced when drought stress was included as a treatment. The challenge associated with classifying belowground stress conditions using aboveground spectral data may be dependent on the emergence of physiological changes in aboveground vegetation [30]. If a sufficient response in the aboveground vegetation is not present, then spectral data may not be able to detect the response and, ultimately, the stress event. Moreover, if an additional stressor elicits a stronger response, the ability of spectral data to identify one individual stress event might be reduced. In the current study, drought elicited stronger physiological responses and had more pronounced relationships with spectral data than the WCR. Our findings suggest that

relying only on vegetation spectral data, including many common indices, to detect WCR infestations might not be appropriate in variable environments.

While the MCARI and PBI responded to WCR infestation under exceptionally controlled conditions (i.e., AAPF experiment), they either did not respond in a less homogenous environment with multiple stressors occurring (i.e., the MCARI in the GH) or the response magnitude was dependent on the presence or absence of water stress (i.e., the PBI in the GH). In the GH experiment, the DSWI did vary among the WCR treatments, but the response was also dependent on the presence or absence of water stress conditions. Combined outcomes from the index data suggest that specific conditions might be required for WCR detection using spectral data. While some studies have shown the ability of indices to use aboveground spectral data to detect belowground stress responses in plants [35–40], others have found that even aboveground herbivory in maize might not be detected using foliar measurements [26]. In the current study, the combination of multiple stressors appears to influence the detection of an individual stress event, with the outcome dependent on the magnitude of the response to the cooccurring stressor.

Drought masking the presence of WCR might also be expected, because drought has been shown to potentially trigger stronger physiological responses in the area measurements were collected (i.e., foliage) relative to the belowground herbivory by WCR [65]. While other studies have found that a reduction in CO<sub>2</sub> assimilation occurs in maize under WCR infestation [66], we found few differences in multiple gas exchange and water-related functional responses (e.g., net CO<sub>2</sub> assimilation and water potential) in the absence of drought stress. The changes in these functional responses were detected only under drought stress. While we did find an increase in leaf temperature in response to WCR infestation, the response varied between genotypes, with the resistant genotype not experiencing as large a leaf temperature increase. Conversely, drought stress elicited much stronger physiological responses, such as reducing net CO<sub>2</sub> assimilation, transpiration rates, and stomatal conductance. These results support those of others that show that drought stress can have a greater negative impact on maize physiology than WCR infestation [17,18]. The stronger the influence of drought compared to WCR on spectral features was further confirmed by relationships between the NDSI values and treatment combinations between the two experiments. Combined, these outcomes highlight the challenges of simultaneously classifying multiple sources of stress [30], especially those that demonstrate a range of physiological responses.

## 5. Conclusions

In summary, we found that, while aboveground composite spectral profiles separated between maize infested or not infested with WCR, classification was poor, and water stress influenced the magnitude of separation of composite spectral profiles. These outcomes were likely based on the differences in the physiological responses of maize to the different stressors, with the vegetation indices and physiological responses to drought more pronounced. While the use of aboveground vegetation optical properties to detect belowground pests and pathogens could be beneficial in most crop production systems, our results highlight an important knowledge gap to be faced when using hyperspectral data to detect and classify specific stress events in plants under variable environmental conditions. Our findings do, however, contribute to the growing literature on using aboveground measurements to detect belowground stress prior to the presence of visible symptoms.

**Author Contributions:** Conceptualization, R.P.-D., L.C., L.S.E. and J.J.C.; methodology, R.P.-D., L.C., L.S.E., M.V.M., C.H.K. and J.J.C.; validation, R.P.-D. and J.J.C.; formal analysis, R.P.-D., A.M. and J.J.C.; investigation, R.P.-D. and J.J.C.; resources, J.J.C. and L.E.; data curation, R.P.-D.; writing—original draft preparation, R.P.-D.; writing—review and editing, R.P.-D., L.C., M.V.M., C. K., L.S.E. and J.J.C.; supervision, J.J.C.; project administration, J.J.C.; and funding acquisition, J.J.C. All authors have read and agreed to the published version of the manuscript.

**Funding:** This work was supported by the Indiana Corn Marketing Council and USDA NIFA Hatch awards IND011490 to J.J.C.

**Data Availability Statement:** Data used in this study are available upon request.

**Acknowledgments:** We would like to thank Marguerite Bolt, Daniel Edwards, Michael Gosney, Megan Haas, Noel Mano, Taylor Nelson, Hannah Quellhorst, Amiee Stramoswski, Anupreet Saini, and Ingrid Xu for the assistance with data collection in the greenhouse. We would also like to thank Chris Hoagland and Yang Yang for assistance with the experimental setup in the Ag Alumni Phenotyping facility and Nathan Deppe and Dan Little for the assistance with plant maintenance in the greenhouse.

**Conflicts of Interest:** The authors declare no conflict of interest.

## Appendix A. Example Image of Root Damage and Analysis of Root Damage



**Figure A1.** Image of both genotypes under WCR infection in the AAPF environment. (a) Genotype resistant to WCR (NGS) and (b) genotype susceptible to WCR (R802).

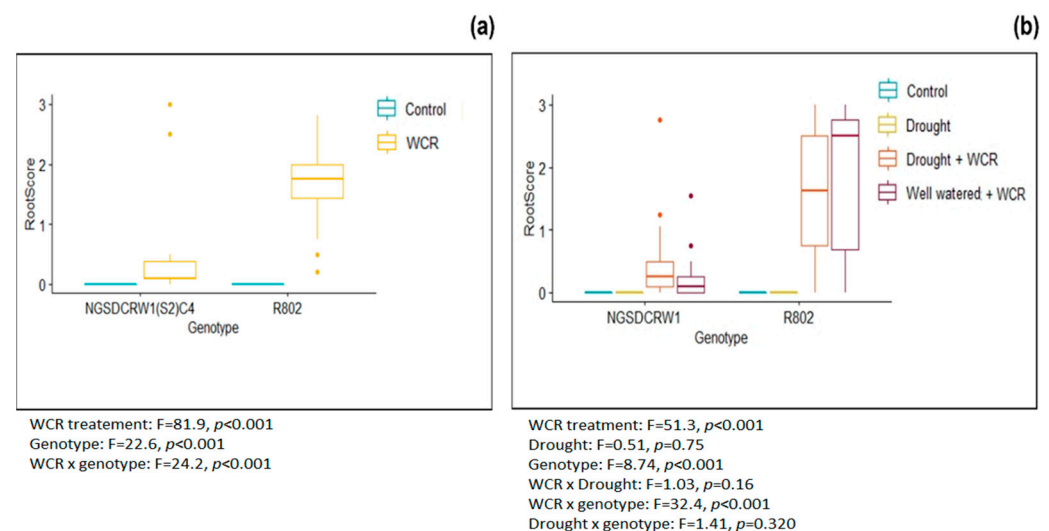


**Figure A2.** Analysis of variance (ANOVA) of node injury scores evaluated following Oleson et al.'s (2005) protocol. Results show plants' distribution of node injury scores at the AAPF experiment (a) and the GH experiment (b). WCR: Western corn rootworm treatment.

**Appendix B. Post Hoc Analysis of Significant PERMANOVA Terms, Vegetation Indices, Chemometric Modeling Performance Metrics, and Functional Trait Values Calculated from the Spectral Data**

**Table A1.** Least squares mean post hoc comparison of statistically significant or marginally statistically significant terms in the PERMANOVA of the spectral profiles from the Ag Alumni Phenotyping Facility (AAPF) or the horticulture greenhouse facility (GH).

Experiment	WCR	posthoc comparison	Genotype	posthoc comparison
AAPF	WCR+	a	NGS	a
	WCR-	b	R802	b

Experiment	Drought	posthoc comparison	Genotype	posthoc comparison	WCR × drought	posthoc comparison	Drought × genotype	posthoc comparison
GH	Drought+	a	NGS	a	WCR-, Drought- WCR+, Drought-	a bc	NGS,0 NGS,1	a b
	Drought-	b	R802	b	WCR-, Drought+ WCR+, Drought+	c c	R802,0 R802,1	a a

**Table A2.** Means ± standard deviation of the indices for the AAPF and GH experiments. AAPF: Ag Alumni controlled environment Phenotyping Facility, GH: greenhouse, PRI: Photochemical reflectance index, NDWI: Normalized Difference Water Index, DSWI: Disease Severity Water Index, PBI: Plant Biochemical Index, ARI: Anthocyanin Reflectance Index, HI: Health Index, WBI: Water Band Index, and MCARI: Modified Chlorophyll Absorption in Reflectance Index.

	Genotype	Treatments	PRI	NDWI	DSWI	PBI	ARI	HI	WBI	MCARI
AAPF	NGS	Control	0.004 ± 0.002	0.046 ± 0.001	4.823 ± 0.103	2.996 ± 0.083	0.334 ± 0.016	0.032 ± 0.005	0.956 ± 0.001	0.154 ± 0.009
		WCR	0.001 ± 0.001	0.044 ± 0.001	4.685 ± 0.092	2.720 ± 0.074	0.317 ± 0.014	0.0321 ± 0.005	0.957 ± 0.001	0.187 ± 0.008
	R802	Control	0.007 ± 0.001	0.048 ± 0.001	4.695 ± 0.090	2.933 ± 0.073	0.329 ± 0.016	0.046 ± 0.005	0.953 ± 0.001	0.161 ± 0.008
		WCR	0.009 ± 0.002	0.049 ± 0.001	4.776 ± 0.106	2.924 ± 0.083	0.324 ± 0.014	0.041 ± 0.006	0.954 ± 0.001	0.168 ± 0.009
GH	NGS	Control	0.019 ± 0.001	0.046 ± 0.002	4.852 ± 0.238	3.760 ± 0.106	0.384 ± 0.025	0.064 ± 0.007	0.954 ± 0.002	0.070 ± 0.003
		WCR	0.016 ± 0.001	0.048 ± 0.002	4.224 ± 0.238	3.362 ± 0.106	0.353 ± 0.025	0.042 ± 0.007	0.953 ± 0.002	0.078 ± 0.003
		Drought	0.009 ± 0.001	0.043 ± 0.001	3.473 ± 0.168	2.903 ± 0.075	0.251 ± 0.018	0.015 ± 0.005	0.957 ± 0.002	0.080 ± 0.002
		WCR + Drought	0.008 ± 0.001	0.045 ± 0.001	3.378 ± 0.168	2.877 ± 0.075	0.233 ± 0.018	0.013 ± 0.005	0.955 ± 0.002	0.077 ± 0.002
	R802	Control	0.018 ± 0.001	0.050 ± 0.002	4.716 ± 0.238	3.445 ± 0.106	0.319 ± 0.025	0.068 ± 0.007	0.949 ± 0.001	0.080 ± 0.003
		WCR	0.017 ± 0.001	0.041 ± 0.001	4.191 ± 0.238	3.199 ± 0.106	0.282 ± 0.025	0.057 ± 0.007	0.951 ± 0.001	0.081 ± 0.003
		Drought	0.015 ± 0.009	0.044 ± 0.001	4.491 ± 0.168	3.425 ± 0.075	0.325 ± 0.018	0.059 ± 0.005	0.957 ± 0.001	0.076 ± 0.002
		WCR + Drought	0.016 ± 0.001	0.044 ± 0.001	4.685 ± 0.170	3.378 ± 0.075	0.337 ± 0.018	0.013 ± 0.005	0.955 ± 0.001	0.083 ± 0.002

**Table A3.** Performance metrics of chemometric models developed using GH data. Number of latent variables (LVs); goodness of fit ( $R^2$ ); root mean square error (RMSE); percent normalized root mean square error (NRMSE); and bias for calibration, cross-validation (CV), and external validation (EV). Calibration cross-validation performance metrics were generated using 100 random permutations of 80% of the total dataset divided into an 80:20 split for calibration and CV, respectively. Performance metrics for EV were generated by applying coefficients generated in the C:CV approach to the 20% of the data excluded. Data shown for C and CV as the mean  $\pm$  standard deviation. Trait abbreviations: A: net CO<sub>2</sub> assimilation ( $\mu\text{mol CO}_2 \text{ m}^{-2} \text{ s}^{-1}$ ), E: transpiration ( $\text{mmol H}_2\text{O m}^{-2} \text{ s}^{-1}$ ),  $g_s$ : stomatal conductance ( $\text{mol H}_2\text{O m}^{-2} \text{ s}^{-1}$ ), RWC: relative water content (%),  $C_i$ : intercellular CO<sub>2</sub> concentration ( $\mu\text{mol CO}_2 \text{ mol air}^{-1}$ ),  $T_{\text{leaf}}$ : leaf temperature ( $^{\circ}\text{C}$ ), SLA: specific leaf area ( $\text{cm mg}^{-1}$ ), WUE: water use efficiency ( $\mu\text{mol CO}_2 \text{ mol}^{-1} \text{ H}_2\text{O}$ ), LWP: leaf water potential (MPa), LOP: leaf osmotic potential (MPa), and leaf greenness (SPAD): estimate of chlorophyll. Models used for the estimates of functional trait responses are in bold.

Trait	LV	Calibration				CV				EV			
		$R^2$	RMSE	NRMSE (%)	Bias	$R^2$	RMSE	NRMSE (%)	Bias	$R^2$	RMSE	NRMSE (%)	Bias
A	17	0.94 $\pm$ 0.00	3.71 $\pm$ 0.13	8.5	$1.05 \times 10^{-14} \pm 0.00$	0.84 $\pm$ 0.04	6.21 $\pm$ 0.68	14.3	0.311 $\pm$ 1.21	0.77	8.07	18.1	0.66
E	15	0.90 $\pm$ 0.00	0.47 $\pm$ 0.01	9.7	$-1.5 \times 10^{-16} \pm 0.00$	0.79 $\pm$ 0.05	0.68 $\pm$ 0.07	14.1	0.003 $\pm$ 0.13	0.65	1.03	18.1	0.04
$g_s$	17	0.90 $\pm$ 0.00	0.05 $\pm$ 0.00	7.6	$1.39 \times 10^{-17} \pm 0.00$	0.75 $\pm$ 0.05	0.08 $\pm$ 0.00	12.8	0.001 $\pm$ 0.01	0.65	0.1	20.4	-0.01
RWC	15	0.91 $\pm$ 0.01	0.04 $\pm$ 0.00	5.3	$3.89 \times 10^{-18} \pm 0.00$	0.79 $\pm$ 0.08	0.06 $\pm$ 0.01	7.6	0.001 $\pm$ 0.01	0.86	0.05	9.8	-0.01
$C_i$	18	0.94 $\pm$ 0.05	18.36 $\pm$ 0.69	6.5	$-6.2 \times 10^{-15} \pm 0.00$	0.84 $\pm$ 0.05	30.02 $\pm$ 3.23	10.6	0.379 $\pm$ 5.01	0.73	47.36	16.1	-1.93
$T_{\text{leaf}}$	19	0.96 $\pm$ 0.00	0.47 $\pm$ 0.01	5.1	$1.3 \times 10^{-16} \pm 0.00$	0.88 $\pm$ 0.03	0.86 $\pm$ 0.10	9.3	-0.026 $\pm$ 0.16	0.71	1.31	14.6	0.39
SLA	13	0.78 $\pm$ 0.02	22.3 $\pm$ 0.83	4.4	$-6.18 \times 10^{-16} \pm 0.00$	0.60 $\pm$ 0.09	31.8 $\pm$ 3.58	6.2	0.082 $\pm$ 6.89	0.67	28.56	5.7	1.98
WUE	17	0.85 $\pm$ 0.01	14.50 $\pm$ 0.45	10.6	$1.1 \times 10^{-14} \pm 0.00$	0.65 $\pm$ 0.09	22.77 $\pm$ 2.08	17.6	-0.534 $\pm$ 4.57	0.50	30.99	34.3	3.57
LWP	9	0.78 $\pm$ 0.01	2.48 $\pm$ 0.07	3.5	$-3.8 \times 10^{-16} \pm 0.00$	0.71 $\pm$ 0.06	2.91 $\pm$ 0.30	4.1	-0.038 $\pm$ 0.61	0.50	4.07	20.4	0.42
LOP	17	0.84 $\pm$ 0.02	49.71 $\pm$ 1.50	5.4	$5.51 \times 10^{-14} \pm 0.00$	0.64 $\pm$ 0.11	78.72 $\pm$ 6.36	8.6	-1.880 $\pm$ 12.51	0.47	85.52	16.0	7.32
SPAD	11	0.73 $\pm$ 0.01	2.41 $\pm$ 0.06	8.4	$-1.7 \times 10^{-18} \pm 0.00$	0.61 $\pm$ 0.09	2.93 $\pm$ 0.28	10.3	-0.060 $\pm$ 0.56	0.33	4.62	20.2	0.48

**Table A4.** Means  $\pm$  standard deviation of the traits for the AAPF and GH experiments. AAPF: Ag Alumni controlled environment Phenotyping Facility, A: net CO<sub>2</sub> assimilation ( $\mu\text{mol CO}_2 \text{ m}^{-2} \text{ s}^{-1}$ ), Transp: transpiration ( $\text{mmol H}_2\text{O m}^{-2} \text{ s}^{-1}$ ),  $C_i$ : intercellular CO<sub>2</sub> concentration ( $\mu\text{mol CO}_2 \text{ mol air}^{-1}$ ), RWC: relative water content (%),  $T_{\text{leaf}}$ : leaf temperature ( $^{\circ}\text{C}$ ), Cond: stomatal conductance ( $\text{mol H}_2\text{O m}^{-2} \text{ s}^{-1}$ ), and SLA: specific leaf area ( $\text{cm mg}^{-1}$ ).

	Genotype	Treatments	A	Transp	$C_i$	RWC	$T_{\text{leaf}}$	Cond	SLA
			AAPF	NGS	Control	10.4 $\pm$ 4.9	0.63 $\pm$ 0.7	273.3 $\pm$ 33.2	0.79 $\pm$ 0.06
		WCR	7.7 $\pm$ 4.9	0.23 $\pm$ 0.7	302.9 $\pm$ 33.2	0.71 $\pm$ 0.06	28.4 $\pm$ 0.2	-0.09 $\pm$ 0.06	309.9 $\pm$ 28.5
	R802	Control	10.0 $\pm$ 4.9	0.76 $\pm$ 0.6	264.0 $\pm$ 31.8	0.84 $\pm$ 0.05	30.0 $\pm$ 0.2	-0.06 $\pm$ 0.05	413.0 $\pm$ 28.95
		WCR	7.5 $\pm$ 4.9	0.63 $\pm$ 0.7	314.1 $\pm$ 33.2	0.76 $\pm$ 0.06	30.5 $\pm$ 0.2	-0.14 $\pm$ 0.06	405.7 $\pm$ 28.9

Table A4. Cont.

	Genotype	Treatments	A	Transp	C <sub>i</sub>	RWC	Tleaf	Cond	SLA
GH	NGS	Control	37.1 ± 2.2	3.98 ± 0.2	156.5 ± 15.2	0.95 ± 0.02	28.5 ± 0.5	0.37 ± 0.02	364.8 ± 17.4
		WCR	36.9 ± 2.1	3.80 ± 0.2	147.0 ± 14.8	0.95 ± 0.02	528.5 ± 0.5	0.35 ± 0.02	424.1 ± 11.9
		Drought	5.1 ± 1.5	0.63 ± 0.1	305.9 ± 10.5	0.68 ± 0.01	28.5 ± 0.4	0.05 ± 0.01	390.7 ± 16.8
		WCR + Drought	6.96 ± 1.5	0.79 ± 0.1	272.4 ± 10.5	0.70 ± 0.01	28.7 ± 0.4	0.06 ± 0.01	397.9 ± 11.9
	R802	Control	37.5 ± 2.1	4.01 ± 0.2	165.4 ± 14.8	0.94 ± 0.02	28.0 ± 0.5	0.40 ± 0.02	378.3 ± 16.8
		WCR	33.3 ± 2.1	3.71 ± 0.2	164.9 ± 14.8	0.95 ± 0.02	28.6 ± 0.5	0.33 ± 0.02	422.1 ± 11.9
		Drought	17.4 ± 1.5	1.82 ± 0.1	181.1 ± 10.6	0.88 ± 0.01	28.1 ± 0.4	0.16 ± 0.01	411.0 ± 16.7
		WCR+Drought	18.1 ± 1.5	1.93 ± 0.1	181.1 ± 10.6	0.90 ± 0.01	28.5 ± 0.4	0.16 ± 0.01	433.6 ± 12.2

## References

1. Conklin, A.R.; Stilwell, T. (Eds.) Grain Crops. In *World Food: Production and Use*; Wiley: Hoboken, NJ, USA, 2007; pp. 77–127.
2. Shiferaw, B.; Prasanna, B.M.; Hellin, J.; Bänziger, M. Crops that feed the world 6. Past successes and future challenges to the role played by maize in global food security. *Food Secur.* **2011**, *3*, 307–327. [[CrossRef](#)]
3. Erenstein, O.; Jaleta, M.; Sonder, K.; Mottaleb, K.; Prasanna, B.M. Global maize production, consumption and trade: Trends and R&D implications. *Food Secur.* **2022**, *14*, 1295–1319.
4. FAO. Statistical Yearbook of the Food and Agricultural Organization for Feeding the World. In *FAO Statistical Yearbook 2013*. 2013. Available online: [www.fao.org/giews/english/fo/index.htm](http://www.fao.org/giews/english/fo/index.htm) (accessed on 15 February 2019).
5. Spencer, J.L.; Hibbard, B.E.; Moeser, J.; Onstad, D.W. Behavior and ecology of the western corn rootworm (*Diabrotica virgifera virgifera* LeConte). *Agric. For. Entomol.* **2009**, *11*, 9–27.
6. Rice, M.E. Transgenic rootworm corn: Assessing potential agronomic, economic, and environmental benefits. *Plant Health Prog.* **2004**, *5*, 12. [[CrossRef](#)]
7. Wechsler, S.; Smith, D. Has resistance taken root in US corn fields? Demand for insect control. *Am. J. Agric. Econ.* **2018**, *100*, 1136–1150. [[CrossRef](#)]
8. Tinsley, N.A.; Estes, R.E.; Gray, M.E. Validation of a nested error component model to estimate damage caused by corn rootworm larvae. *J. Appl. Entomol.* **2013**, *137*, 161–169. [[CrossRef](#)]
9. Jakka, S.R.K.; Shrestha, R.B.; Gassmann, A.J. Broad-spectrum resistance to *Bacillus thuringiensis* toxins by western corn rootworm (*Diabrotica virgifera virgifera*). *Sci. Rep.* **2016**, *6*, 27860. [[CrossRef](#)] [[PubMed](#)]
10. Cullen, E.M.; Gray, M.E.; Gassmann, A.J.; Hibbard, B.E. Resistance to Bt corn by western corn rootworm (Coleoptera: Chrysomelidae) in the U.S. Corn Belt. *J. Integr. Pest Manag.* **2013**, *4*, D1–D6. [[CrossRef](#)]
11. Gassmann, A.J.; Shrestha, R.B.; Jakka, S.R.K.; Dunbar, M.W.; Clifton, E.H.; Paolino, A.R.; Ingber, D.A.; French, B.W.; Masloski, K.E.; Dounda, J.W.; et al. Evidence of resistance to Cry34/35Ab1 corn by western corn rootworm (Coleoptera: Chrysomelidae): Root injury in the field and larval survival in plant-based bioassays. *J. Econ. Entomol.* **2016**, *109*, 1872–1880. [[CrossRef](#)]
12. Gassmann, A.J.; Petzold-Maxwell, J.L.; Keweshan, R.S.; Dunbar, M.W. Western corn rootworm and Bt maize. *GM Crops Food* **2012**, *3*, 235–244. [[CrossRef](#)]
13. Moar, W.; Khajuria, C.; Pleau, M.; Ilagan, O.; Chen, M.; Jiang, C.; Prics, P.; McNulty, B.; Clark, T.; Head, G. Cry3Bb1-Resistant western corn rootworm, *Diabrotica virgifera virgifera* (LeConte) does not exhibit cross-resistance to DvSnf7 dsRNA. *PLoS ONE* **2017**, *12*, e0169175. [[CrossRef](#)]
14. Sankaran, S.; Mishra, A.; Ehsani, R.; Davis, C. A review of advanced techniques for detecting plant diseases. *Comput. Electron. Agric.* **2010**, *72*, 1–13. [[CrossRef](#)]
15. Nowatzki, T.M.; Tollefson, J.J.; Calvin, D.D. Development and validation of models for predicting the seasonal emergence of corn rootworm (Coleoptera: Chrysomelidae) beetles in Iowa. *Environ. Entomol.* **2002**, *31*, 864–873. [[CrossRef](#)]
16. Aslam, M.; Maqbool, M.A.; Cengiz, R. *Drought stress in Maize (Zea Mays L.)*; Springer International Publishing: Cham, Switzerland, 2015.
17. Mahmoud, A.M.B. Effects of Western Corn Rootworm Larval Feeding, Drought, and Their Interaction on Maize Performance and Rootworm Development. Ph.D. Thesis, University of Missouri, Columbia, MO, USA, 2015.
18. Mahmoud, M.A.B.; Sharp, R.E.; Oliver, M.J.; Finke, D.L.; Bohn, M.; Ellersieck, M.R.; Hibbard, B.E. Response of maize hybrids with and without rootworm- and drought-tolerance to rootworm infestation under well-watered and drought conditions. *J. Econ. Entomol.* **2018**, *111*, 193–208. [[CrossRef](#)] [[PubMed](#)]
19. Mahmoud, M.A.B.; Sharp, R.E.; Oliver, M.J.; Finke, D.L.; Ellersieck, M.R.; Hibbard, B.E. The effect of western corn rootworm (Coleoptera: Chrysomelidae) and water deficit on maize performance under controlled conditions. *J. Econ. Entomol.* **2016**, *10*, 684–698. [[CrossRef](#)]
20. Mahlein, A.-K.; Steiner, U.; Hillnhütter, C.; Dehne, H.-W.; Oerke, E.-C. Hyperspectral imaging for small-scale analysis of symptoms caused by different sugar beet diseases. *Plant Methods* **2012**, *8*, 3. [[CrossRef](#)] [[PubMed](#)]
21. Mutka, A.M.; Bart, R.S. Image-based phenotyping of plant disease symptoms. *Front. Plant Sci.* **2015**, *5*, 734. [[CrossRef](#)]
22. Cotrozzi, L.; Couture, J.J.; Cavender-Bares, J.; Kingdon, C.C.; Fallon, B.; Pilz, G.; Pellegrini, E.; Nalia, C.; Townsend, P.A. Using foliar spectral properties to assess the effects of drought on plant water potential. *Tree Physiol.* **2017**, *184*, 1582–1591. [[CrossRef](#)]
23. Susič, N.; Žibrat, U.; Širca, S.; Strajnar, P.; Razinger, J.; Knapič, M.; Vončina, M.; Urek, G.; Gerič Stare, B. Discrimination between abiotic and biotic drought stress in tomatoes using hyperspectral imaging. *Sens. Actuators B Chem.* **2018**, *273*, 842–852. [[CrossRef](#)]
24. Zarco-Tejada, P.J.; Camino, C.; Beck, P.S.A.; Calderon, R.; Hornero, A.; Hernández-Clemente, R.; Kattenborn, T.; Montes-Borrego, B.; Susca, L.; Morelli, M.; et al. Previsual symptoms of *Xylella fastidiosa* infection revealed in spectral plant-trait alterations. *Nat. Plants* **2018**, *4*, 432–439. [[CrossRef](#)]
25. Couture, J.J.; Singh, A.; Charkowski, A.O.; Groves, R.L.; Gray, S.M.; Bethke, P.C.; Townsend, P.A. Integrating spectroscopy with potato disease management. *Plant Dis.* **2018**, *102*, 2233–2240. [[CrossRef](#)] [[PubMed](#)]
26. do Prado Ribeiro, L.; Klock, A.L.S.; Filho, J.A.W.; Tramontin, M.A.; Trapp, M.A.; Mithöfer, A.; Nansen, C. Hyperspectral imaging to characterize plant-plant communication in response to insect herbivory. *Plant Methods* **2018**, *14*, 54. [[CrossRef](#)] [[PubMed](#)]
27. Nagasubramanian, K.; Jones, S.; Sarkar, S.; Singh, A.K.; Singh, A.; Ganapathysubramanian, B. Hyperspectral band selection using genetic algorithm and support vector machines for early identification of charcoal rot disease in soybean stems. *Plant Methods* **2018**, *14*, 86. [[CrossRef](#)] [[PubMed](#)]

28. Campos-Medina, V.A.; Cotrozzi, L.; Stuart, J.J.; Couture, J.J. Spectral characterization of wheat functional trait responses to Hessian fly: Mechanisms for trait-based resistance. *PLoS ONE* **2019**, *14*, e0219431. [[CrossRef](#)]
29. Yao, Z.; Lei, Y.; He, D. Early visual detection of wheat stripe rust using visible/near-infrared hyperspectral imaging. *Sensors* **2019**, *19*, 952. [[CrossRef](#)]
30. Cotrozzi, L.; Couture, J.J. Hyperspectral assessment of plant responses to multi-stress environments: Prospects for managing protected agrosystems. *Plants People Planet* **2020**, *2*, 244–258. [[CrossRef](#)]
31. Fallon, B.; Yang, A.; Lapadat, C.; Armour, I.; Juzwik, J.; Montgomery, R.A.; Cavender-Bares, J. Spectral differentiation of oak wilt from foliar fungal disease and drought is correlated with physiological changes. *Tree Physiol.* **2020**, *40*, 377–390. [[CrossRef](#)]
32. Gold, K.M.; Townsend, P.A.; Chlus, A.; Herrmann, I.; Couture, J.J.; Larson, E.R.; Gevens, A.J. Hyperspectral measurements enable pre-symptomatic detection and differentiation of contrasting physiological effects of late blight and early blight in potato. *Remote Sens.* **2020**, *12*, 286. [[CrossRef](#)]
33. Gold, K.M.; Townsend, P.A.; Herrmann, I.; Gevens, A.J. Investigating potato late blight physiological differences across potato cultivars with spectroscopy and machine learning. *Plant Sci.* **2020**, *295*, 110316. [[CrossRef](#)]
34. Pérez-Roncal, C.; López-Maestresalas, A.; Lopez-Molina, C.; Jarén, C.; Urrestarazu, J.; Santesteban, L.G.; Arazuri, S. Hyperspectral imaging to assess the presence of powdery mildew (*Erysiphe necator*) in cv. Carignan noir grapevine bunches. *Agronomy* **2020**, *10*, 88. [[CrossRef](#)]
35. Calamita, F.; Imran, H.A.; Vescovo, L.; Mekhalfi, M.L.; La Porta, N. Early identification of root rot disease by using hyperspectral reflectance: The case of pathosystem grapevine/armillaria. *Remote Sens.* **2021**, *13*, 2436. [[CrossRef](#)]
36. Reynolds, G.J.; Windels, C.E.; MacRae, I.V.; Laguette, S. Remote sensing for assessing rhizoctonia crown and root rot severity in sugar beet. *Plant Dis.* **2012**, *96*, 497–505. [[CrossRef](#)]
37. Pozdnyakova, L.; Oudemans, P.V.; Hughes, M.G.; Giménez, D. Estimation of spatial and spectral properties of phytophthora root rot and its effects on cranberry yield. *Comput. Electron. Agric.* **2003**, *37*, 57–70. [[CrossRef](#)]
38. Omer, M.; Locke, J.C.; Frantz, J.M. Using leaf temperature as a nondestructive procedure to detect root rot stress in geranium. *HortTechnology* **2015**, *17*, 532–536. [[CrossRef](#)]
39. Wang, X.; Zhang, M.; Zhu, J.; Geng, S. Spectral prediction of *Phytophthora infestans* infection on tomatoes using artificial neural network (ANN). *Int. J. Remote Sens.* **2008**, *29*, 1693–1706. [[CrossRef](#)]
40. Weksler, S.; Rozenstein, O.; Haish, N.; Moshelion, M.; Wallach, R.; Ben-dor, E. Pepper plants leaf spectral reflectance changes as a result of root rot damage. *Remote Sens.* **2021**, *13*, 980. [[CrossRef](#)]
41. Penuelas, J.; Filella, I.; Gamon, J.A. Assessment of photosynthetic radiation-use efficiency with spectral reflectance. *New Phyt.* **1995**, *131*, 291–296. [[CrossRef](#)]
42. Gao, B.-C. NDWI—A normalized difference water index for remote sensing of vegetation liquid water from space. *Remote Sens. Env.* **1996**, *58*, 257–266. [[CrossRef](#)]
43. Apan, A.; Held, A.; Phinn, S.; Markley, J. Detecting sugarcane “orange rust” disease using EO1 Hyperion hyperspectral imagery. *Inter. J. Remote Sens.* **2004**, *25*, 489–498. [[CrossRef](#)]
44. Rama Rao, N.; Garg, P.; Ghosh, S.; Dadhwal, V. Estimation of leaf total chlorophyll and nitrogen concentrations using hyperspectral satellite imagery. *J. Agri. Sci.* **2008**, *146*, 65–75. [[CrossRef](#)]
45. Gitelson, A.A.; Merzlyak, M.N.; Chivkunova, O.B. Optical properties and nondestructive estimation of anthocyanin content in plant leaves. *Photochem Photobiol.* **2001**, *74*, 38–45. [[CrossRef](#)]
46. Mahlein, A.-K.; Rumpf, T.; Welke, P.; Dehne, H.-W.; Plümer, L.; Steiner, U.; Oerke, E.-C. Development of spectral indices for detecting and identifying plant diseases. **2013**, *128*, 21–30. [[CrossRef](#)]
47. Penuelas, J.; Filella, I.; Biel, C.; Serrano, L.; Savé, R. The reflectance at 950–970 nm region as an indicator of plant water status. *Inter. J. Remote Sens.* **1993**, *14*, 1887–1905. [[CrossRef](#)]
48. Daughtry, C.S.T.; Walthall, C.L.; Kim, M.S.; de Colstoun, E.B.; McMurtery, J.E., III. Estimating corn leaf chlorophyll concentration from leaf and canopy reflectance. *Remote Sens. Environ.* **2000**, *74*, 229–239. [[CrossRef](#)]
49. Stanton, K.M.; Mickelbart, M.V. Maintenance of water uptake and reduced water loss contribute to water stress tolerance of *Spiraea alba* Du Roi and *Spiraea tomentosa* L. *Hort. Res.* **2014**, *1*, 14033. [[CrossRef](#)]
50. Wold, S.; Ruhe, A.; Wold, H.; Dunn, W. The collinearity problem in linear regression: The partial least squares (PLS) approach to generalized inverses. *SIAM J. Sci. Stat. Comput.* **1984**, *5*, 735–743. [[CrossRef](#)]
51. Wold, S.; Sjöström, M.; Eriksson, L. PLS-regression: A basic tool of chemometrics. *Chemom. Intell. Lab. Syst.* **2001**, *58*, 109–130. [[CrossRef](#)]
52. Grossman, Y.L.; Ustin, S.L.; Jacquemoud, S.; Sanders, E.W.; Schmuck, G.; Verdebout, J. Critique of stepwise multiple linear regression for the extraction of leaf biochemistry information from leaf reflectance data. *Remote Sens. Environ.* **1996**, *56*, 182–193. [[CrossRef](#)]
53. Chen, S.; Hong, X.; Harris, C.J.; Sharkey, P.M. Sparse modeling using orthogonal forward regression with PRESS statistic and regularization. *IEEE Trans. Syst. Man Cybern. Part B* **2004**, *34*, 898–911. [[CrossRef](#)] [[PubMed](#)]
54. Oleson, J.D.; Park, Y.L.; Nowatzki, T.M.; Tollefson, J.J. Node-injury scale to evaluate root injury by corn rootworms (Coleoptera: Chrysomelidae). *J. Econ. Entomol.* **2005**, *98*, 1–8. [[CrossRef](#)]
55. Anderson, M.J. A new method for non-parametric multivariate analysis of variance. *Austral Ecol.* **2001**, *26*, 32–46.

56. Rumpf, T.; Mahlein, A.K.; Steiner, U.; Oerke, E.C.; Dehne, H.W.; Plümer, L. Early detection and classification of plant diseases with Support Vector Machines based on hyperspectral reflectance. *Comput. Electron. Agric.* **2010**, *74*, 91–99. [[CrossRef](#)]
57. Fillion, M.; Dutilleul, P.; Potvin, C. Optimum experimental design for free-air carbon dioxide enrichment (FACE) studies. *Glob. Chang. Biol.* **2000**, *6*, 843–854. [[CrossRef](#)]
58. Galiene, A.; D’Ascenzo, N.; Stagnari, F.; Pagnani, G.; Xie, Q.; Pisante, M. Past and future of plant stress detection: An overview from remote sensing to positron emission tomography. *Front. Plant Sci.* **2021**, *11*, 609155. [[CrossRef](#)] [[PubMed](#)]
59. Kashyap, B.; Kumar, R. Sensing methodologies in agriculture for monitoring biotic stress in plants due to pathogens and pests. *Inventions* **2021**, *6*, 29. [[CrossRef](#)]
60. Lowe, A.; Harrison, N.; French, A.P. Hyperspectral image analysis techniques for the detection and classification of the early onset of plant disease and stress. *Plant Methods* **2017**, *13*, 80. [[CrossRef](#)]
61. Abdulridha, J.; Ehsani, R.; Abd-Elrahman, A.; Ampatzidis, Y. A remote sensing technique for detecting laurel wilt disease in avocado in presence of other biotic and abiotic stresses. *Comput. Electron. Agric.* **2019**, *156*, 549–557. [[CrossRef](#)]
62. Bravo, C.; Moshou, D.; West, J.; McCartney, A.; Ramon, H. Early disease detection in wheat fields using spectral reflectance. *Biosyst. Eng.* **2003**, *84*, 137–145. [[CrossRef](#)]
63. Moshou, D.; Bravo, C.; West, J.; Wahlen, T.; McCartney, A.; Ramon, H. Automatic detection of ‘yellow rust’ in wheat using reflectance measurements and neural networks. *Comput. Electron. Agric.* **2004**, *44*, 173–188. [[CrossRef](#)]
64. Wang, D.; Kurle, J.E.; Estevez De Jensen, C.; Percich, J.A. Radiometric assessment of tillage and seed treatment effect on soybean root rot caused by *Fusarium* spp. in central Minnesota. *Plant Soil* **2004**, *258*, 319–331. [[CrossRef](#)]
65. Chávez-Arias, C.C.; Ligarreto-Moreno, G.A.; Ramírez-Godoy, A.; Restrepo-Díaz, H. Maize responses challenged by drought, elevated daytime temperature and arthropod herbivory stresses: A physiological, biochemical and molecular view. *Front. Plant Sci.* **2021**, *12*, 702841. [[CrossRef](#)] [[PubMed](#)]
66. Riedell, W.E.; Reese, R.N. Maize morphology and shoot CO<sub>2</sub> assimilation after root damage by western corn rootworm larvae. *Crop Sci.* **1999**, *39*, 1332–1340. [[CrossRef](#)]

**Disclaimer/Publisher’s Note:** The statements, opinions and data contained in all publications are solely those of the individual author(s) and contributor(s) and not of MDPI and/or the editor(s). MDPI and/or the editor(s) disclaim responsibility for any injury to people or property resulting from any ideas, methods, instructions or products referred to in the content.